ISSN: 1813-4890

Application of Ground Penetrating Radar Simulation and Interpretation Methods for Leakage in Underground Water Supply Pipelines

Chengpeng Ge [a], Yuxin Lu [b] and Guoqi Dong [c]

China University of Mining and Technology (Beijing) 100083, China;

[a]2484594362@qq.com, [b]1419425187@qq.com, [c]2410693539@qq.com

Abstract

For the radar detection of underground water supply pipeline leakage, based on the study of pipeline leakage diffusion law and the influence of surrounding soil water content change on soil dielectric constant, Geo-Studio software is used to establish the leakage model of underground water supply pipeline with different leakage direction and leakage time, and combined with the FDTD to simulate the different models of the GPR orthogonal simulation, to analyze the reflected waves generated in the process of pipeline leakage, The electromagnetic wave field characteristics of the typical pipeline disease model are analyzed under the interference of multiple waves generated during the pipeline leakage process. The results of the study provide a strong support for improving the effectiveness and accuracy of the interpretation of radar detection data for underground water supply pipes and their leakage.

Keywords

Ground-penetrating radar, pipeline leakage, numerical simulation, characterization.

1. Introduction

As an important part of urban infrastructure, the normal operation of underground water supply pipelines is related to the life of the whole city and the production and development of enterprises [1]. However, corrosion of pipes during long-term use leads to frequent ruptures and leaks. Leakage of water supply pipes can cause changes in the nature of the surrounding soil, with areas of severe leakage having loose soil settling and collapsing, which then crushes the pipes and causes leakage over a larger area; For pipelines with shallow burial depths, the leaking water will flow rapidly to the ground above, which in turn will produce a waterlogged road situation [2].

At present, there are many pipeline leakage detection methods, such as conventional hydrometric analysis, listening to pick up the leakage treatment, random excavation of pipelines and other methods compared to [3]. Ground-penetrating radar is characterized by non-destructive, high efficiency, high imaging resolution, and high penetration [4]. Y. Shen et al [5] have analyzed the attributes of GPR detection data of water supply pipe leakage by using crossover frequency technique and channel integration technique, and the results can effectively reflect the degree of water supply pipe leakage; Lai et al [6] carried out GPR physical simulation detection tests for leakage on the upper side of metal water supply pipes and PVC water supply pipes in sandy materials and analyzed the GPR response characteristics of the 2 types of pipe leakage at different times; Lau et al [7] proposed a method for estimating the electromagnetic wave velocity of the medium in the leakage region based on the hyperbolic characteristics of the water supply pipe and concluded that the electromagnetic wave velocity in the region affected by leakage of the water supply pipe is 5-10% smaller than that without leakage through physical simulation tests; Song Hantao et al [8] calculated the GPR profiles of pipelines in sandy soil strata under the conditions of no filling, oil filling and oil seepage using the time domain based finite difference time domain (FDTD) method, and analyzed the results in detail; Shen Yupeng et al [9] used GPR Max software to simulate the detection of water supply pipe leakage at different depths, pipe diameters, and leakage locations, and proposed an identification basis for GPR to detect underground water supply pipe leakage engineering problems. Therefore, the use of non-destructive testing methods to detect leakage problems in underground water supply pipes is particularly necessary.

However, the existing pipeline leakage disease orthogonal simulation and physical models are relatively simple, the simulated leakage range is very regular, and the difference with the actual situation is large, and the lack of complex orthogonal models in line with the real life. In addition, the criteria for recognizing and interpreting radar images for typical pipeline diseases have not yet been established, bringing great blindness to ground-penetrating radar exploration. To this end, this paper firstly adopts Geo-Studio software to establish underground water supply pipe leakage models under different leakage directions and leakage times, and combines FDTD with GPR orthogonal simulation of different models to analyze the electromagnetic wave field characteristics of typical pipeline disease models under the interference of reflected waves and multiple waves generated in the process of pipeline leakage. The results of the study can provide strong support for the effectiveness of underground pipeline leakage ground-penetrating radar detection and the interpretation of radar detection data.

2. Modeling of seepage areas in water supply pipes

2.1 Leakage-induced seepage patterns around pipes

As the water flow law in the seepage zone due to pipe leakage satisfies Darcy's law for unsaturated soils, the two-dimensional differential control equation for seepage flow can be expressed as:

$$\frac{\partial}{\partial x}\left(k_x \frac{\partial H}{\partial x}\right)+\frac{\partial}{\partial y}\left(k_y \frac{\partial H}{\partial y}\right)+Q=\frac{\partial \theta}{\partial t} \tag{1}$$

where H denotes the total head; kx denotes the permeability coefficient in the x-direction; ky denotes the permeability coefficient in the y-direction; Q denotes the applied flow boundary; θ denotes the water content per unit volume; and t denotes time.

From Equation 1, the difference between the fluid inflow and outflow into and out of the cell at a point in the soil body per unit of time is equal to the change in the total flow rate of the soil body per unit of time, which also indicates that the rate of change in the sum of the externally applied circulation in the x- and y-directions is equal to the rate of change in the water content per unit of volume.

The SEEP/W module in Geo-Studio is derived with constant stress and assumes that the air pressure in the void is maintained at a constant atmospheric pressure for the transient case. Thus, the change in water content per unit volume is simply a function of the amount of change in pore water pressure. The seepage control equation in the SEEP/W finite element formulation is:

$$\frac{\partial}{\partial x}\left(k_x \frac{\partial H}{\partial x}\right)+\frac{\partial}{\partial y}\left(k_y \frac{\partial H}{\partial}\right)+Q=m_w \gamma_w \frac{\alpha H}{\alpha t} \tag{2}$$

where m_w is the slope of the water storage curve; γ_w is the water's bulk weight.

In solving the basic equations for the seepage field of unsaturated soils, the soil-water characteristic curve equations proposed by Van Genuchten were used with the following expressions:

$$\theta = \left[\frac{1}{1+(a\psi)^n}\right]^m \tag{3}$$

where ψ denotes the matrix suction of the soil; m, n, and a are fitting parameters.

The method of estimating the permeability coefficient function used in this paper is Van Genuchten's estimation method with the following expression:

$$k_w = k_s \frac{\left[1 - a\psi^{n-1}\left(1+\left(a\psi^n\right)^{-m}\right)\right]^2}{\left(1+a\psi^n\right)^{\frac{m}{2}}} \tag{4}$$

where ks denotes the coefficient of permeability at saturation.

2.2 Electromagnetic characterization of the leakage area

Underground pipeline after being damaged, water leakage in the pipeline and the surrounding soil mixing, its dielectric constant and other electromagnetic wave characteristics have changed, the leakage area and the original soil appear to be different physical properties. Since the dielectric constant of water is much higher than that of soil particles, soil dielectric constant and conductivity are significantly affected by factors such as soil water content. In order to simulate the value of soil dielectric constant under different water content conditions, the relationship between water content and dielectric constant was obtained using TOPP model as follows:

$$e_r = 3.03 + 9.3q_v + 146q_v^2 - 76.6q_v^3 \tag{5}$$

where "ε_r" denotes the dielectric constant and "θ_v" denotes the volumetric water content.

In soils with low media loss, the electrical conductivity of the soil was exponentially correlated (R2 = 0.75) with the water content of the soil, and the regression equation was:

$$s = 4.504e^{8.2635w} \tag{6}$$

where "σ" denotes the apparent conductivity of the soil and "ω" denotes the volumetric water content.

3. Numerical simulation and analysis of results

Table 1 Leakage simulation conditions

saturated permeability coefficient m/s	saturated water content %	Initial water content %	Pipe Diameter mm	water seepage point	Pipe Burial Depth m	head pressure Kpa
10-6	38	5	200	Top Bottom Lateral	1	50
10-6	38	5	1000	Top Bottom Lateral	1	50

A leakage model of an underground water supply pipe with a size of 4.0 m × 4.0 m was developed. The supply pipe is shown in the blue circle in Figures 1 and 3 below, with the center of the pipe circle at (2.0m,3.0m). By generalizing the stratigraphy to a single soil layer and the background medium to a sandy soil, the effects of different pipe diameters, pipe leakage sites, and different leakage days on the leakage zone were simulated (Table 1). The volumetric water content of the sandy soil after 1-10 days of seepage at different seepage locations is shown below in Figs. 1 and 3, a-d, respectively. As can be seen from the figure, when the water supply pipe leaks, the leakage location is different, the formation of the leakage area morphology is different.

The spatial grid is 0.01m × 0.01m, truncated by the PML absorption boundary. As an example, the estimated values of relative dielectric constant and conductivity parameters of sandy soil with 38% water content in the seepage zone were calculated by Eqs. (5) and (6). The water supply pipe is made of PVC and is filled with water internally. The parameters of the forward simulation are set as follows: The transmitting antenna frequency is 300MHz and the Ricker subwave is selected. The moving step is 0.005m. The grid divisions dx, dy, and dz were all 0.01 m, and the time window length was 60 ns. The results of the PVC pipe leakage orthotropy under the condition of 38% water content of sandy soil in the leakage area are shown in Figures 2 and 4.

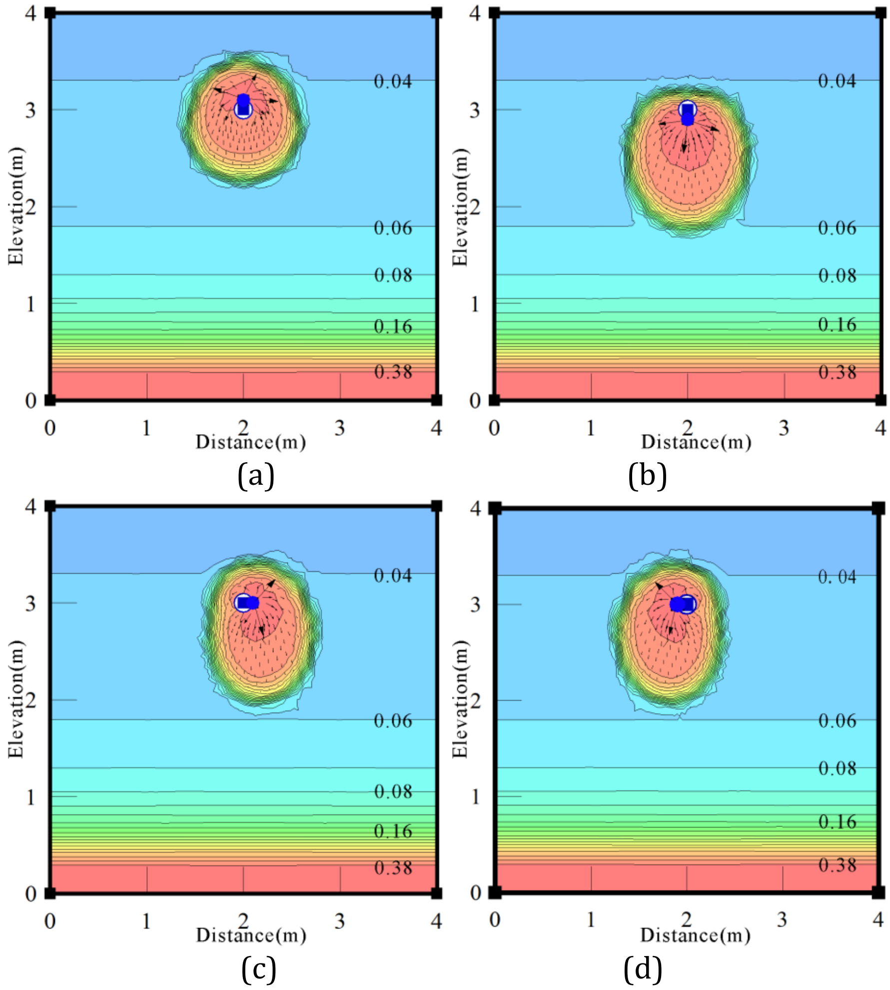

a - top leakage; b - bottom leakage; c - right side leakage; d - left side leakage

Fig. 1 Volumetric water content after 3 days of leakage at different locations of DN=200mm pipe

From Figure 1 above, it can be seen that the shape development characteristics of the leakage zone is closely related to the pipe size, pipe leakage site and the time of leakage. When the pipe diameter is small, the leakage zone can easily cross the pipe and the shape of the leakage zone does not correlate well with the location of the leakage when the leakage time exceeds a certain range.

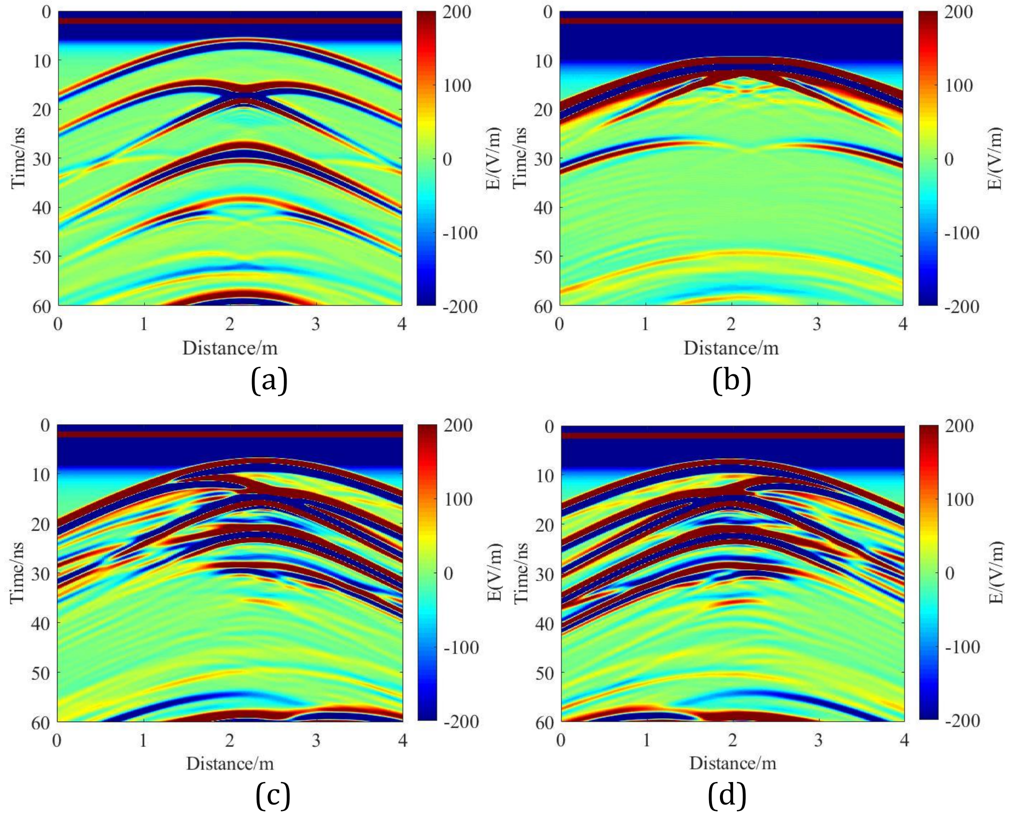

Fig. 2 GPR simulation profiles 3 days after top leakage (a), bottom leakage (b), right leakage (c), and left leakage (d) of DN=200 mm pipe

Fig. 2 shows the GPR simulation profiles of the leakage model at different locations of the 200 mm diameter water supply pipe in Fig. 1. As can be seen from the figure: A hyperbolic wrap-around wave began to appear at the moment of about 4.8 ns at 3 days of leakage on the upper side of the water supply pipe (Fig. 2a). Compared to the 10 ns appearance time of the hyperbolic wrap-around wave for the leakage on the lower side of the water supply pipe in Fig. 2b, the hyperbolic wrap-around wave appears earlier, this is due to the fact that after the leakage on the upper side of the water supply pipe, the area of leakage is close to the surface and the propagation distance becomes smaller. In the leakage on the right side of the water supply pipe in Fig. 2c and on the left side of the water supply pipe in Fig. 2d, the time of appearance of the apex of the hyperbolic wrap-around wave after 3 days of leakage is 7.8 ns. It can be seen that the time of appearance of hyperbolic wrap-around waves is significantly correlated with the location of pipe leakage. When the top and bottom sides of the water supply pipe leak, the apex of the hyperbolic wrap-around wave remains unchanged at the horizontal center. When the water supply pipe leaks on the right and left side, respectively, the apex of the hyperbolic wrap-around wave changes with the location of the leak.

As shown in Figure 3, in order to further analyze the characteristics of the GPR signals at the same time at different leakage locations of the water supply pipe, a single-channel waveform at the horizontal center location of 2.0 m was extracted for comparison. Due to the effect of gravity head, as the leakage time is longer, the sandy soil in the leakage area below the pipe has higher water content and higher conductivity, the electromagnetic wave attenuation is more serious, and the hyperbolic wrap-around wave energy is weaker.

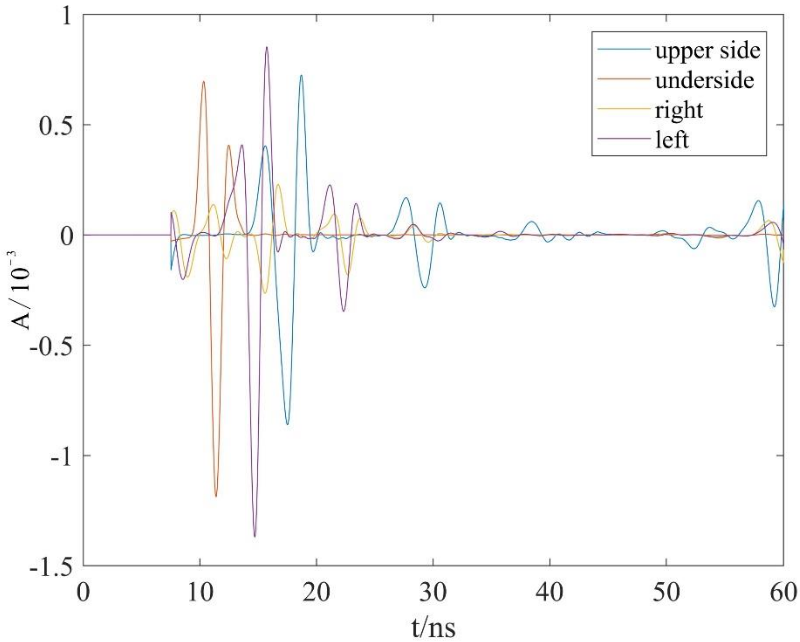

Fig. 3 Comparison of single-channel waveforms at the horizontal center position of DN=200mm pipe leakage

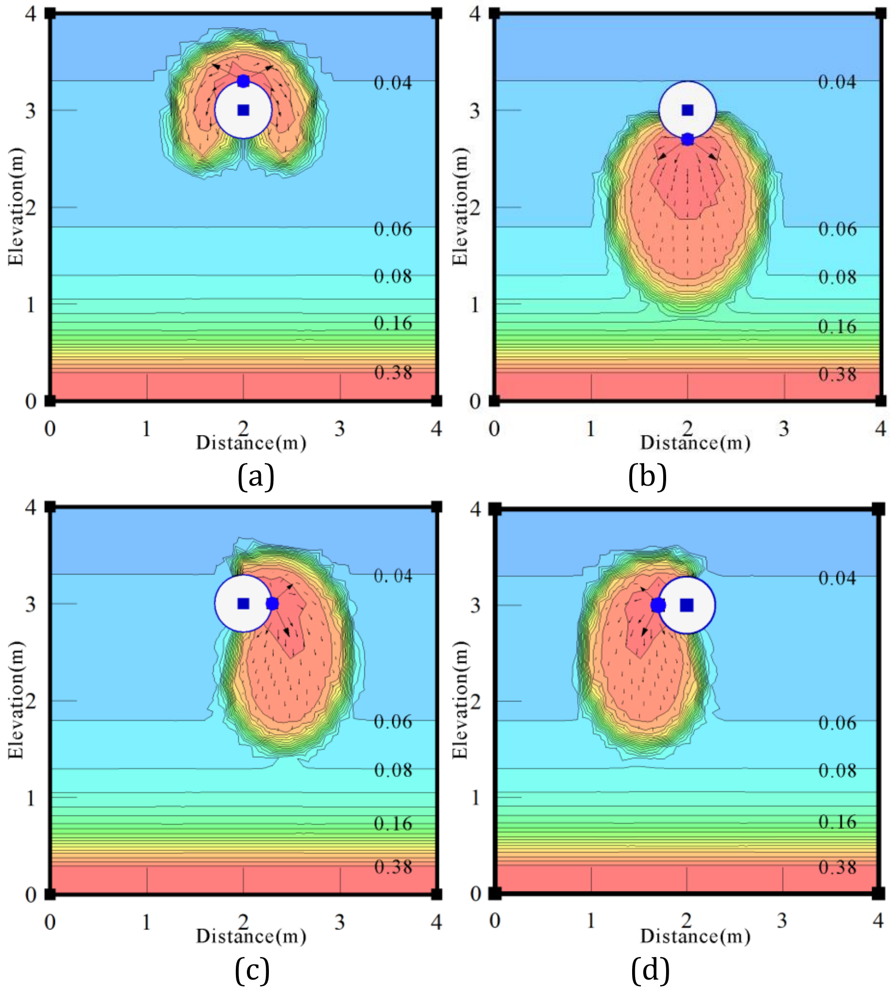

a - top leakage; b - bottom leakage; c - right side leakage; d - left side leakage

Fig. 4 Volumetric water content after 5 days of leakage at different locations of DN=600mm pipe

As can be seen in Figure 4, when the pipe diameter is large, the leakage site has a greater influence on the shape of the leakage zone. When leakage occurs on the side of a large-diameter pipeline, the leakage area is initially developed to the upper part as well as to one side because the water cannot cross the pipeline, and the leakage area develops for a certain period of time, and the water develops across the pipeline towards the other side of the pipeline. At this time, the distribution area of the unsaturated zone increases, and the shape of the leakage zone is more complex; When leakage occurs at the bottom of a large diameter pipe, a leakage zone can form at the bottom because the matrix suction head is not sufficient to overcome the gravity head over the pipe. However the top of the pipe remains in a pristine dry condition and is not affected by the leakage of the pipe. When leakage occurs at the top of a large-diameter pipe, the shape of the leakage area flows downward across the pipe, gradually encircling the entire leakage area of the pipe.

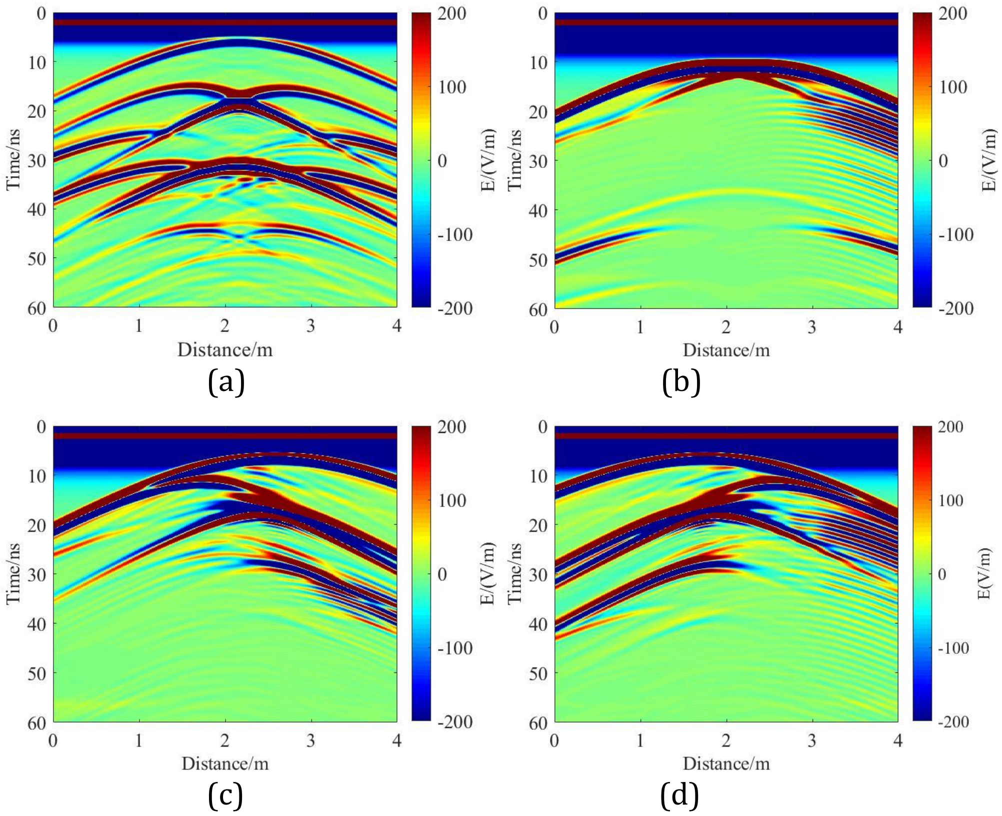

Fig. 5 GPR simulation profiles 5 days after top leakage (a), bottom leakage (b), right side leakage (c), and left side leakage (d) of DN=600 mm pipe

Fig. 5 shows the GPR simulation profiles of the leakage model at different locations of the 600 mm diameter water supply pipe in Fig. 4. As seen in the figure: After 5 days of leakage on the upper side of the water supply pipe, the hyperbolic wrap-around wave begins to appear at about the 3.8 ns moment as shown in Fig. 5a, which is earlier than the appearance of the leakage on the upper side of the water supply pipe after 3 days in Fig. 2a. After 5 days of leakage on the lower side, the weaker and more separated the 2 hyperbolic wrap-around waves are compared to those at 3 days of leakage in Fig. 2b. When the right side leaks for 5 days, a hyperbolic wrap-around wave appears at the horizontal position of 2.8 m at about 8.6 ns, compared with the hyperbolic wrap-around wave at the horizontal position of 2.2 m at 3 days of leakage of a pipe diameter of 200 mm with an appearance time of 9.6 ns. Its apex is clearly shifted to the upper right, and the hyperbolic wrap-around wave appears much earlier. The characteristics of hyperbolic wrap-around wave distribution in the GPR simulated profile for the left leakage are just the opposite of those for the right leakage. The longer the leakage time, the earlier the hyperbolic wrap-around wave appears and the more the apex position is shifted to the upper left side (Fig. 5d).

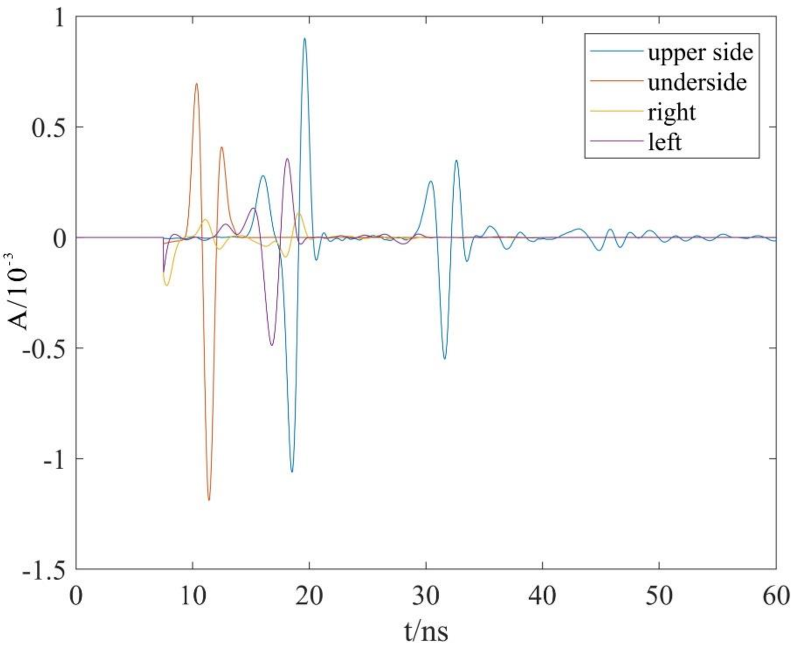

Fig. 6 Comparison of single-channel waveforms at the horizontal center position of DN=600mm pipe leakage

Figure 6 shows a comparison of the single-channel waveforms at the horizontal position in Figure 5. As seen in the figure, the single-channel waveforms selected for leakage at the top and bottom are blue and orange, respectively, and are very significantly affected by leakage. The peaks and valleys of the two single-channel waveforms are more pronounced, and the peaks of the yellow waveform for the left leakage appear earlier than those of the purple waveform for the right leakage, but the four waveforms generally tend to be consistent. As the seepage time gets longer, the higher the water content of the sandy soil, the higher the conductivity, resulting in stronger attenuation of the electromagnetic wave propagating through it and weaker hyperbolic wrap-around wave energy.

4. Conclusion

In this paper, for the problem of GPR detection of leakage in underground water supply pipes, firstly, the water supply pipe leakage model was constructed by using Geo-Studio software. Then GPR numerical simulation profiles were simulated using FDTD for different diameters of water supply pipes and leakage locations for different leakage times at the top, bottom, right side and left side respectively, and analyzed in comparison with GPR physical simulation profiles. The results show: The longer the seepage time, the larger the seepage area, the higher the water content of the sandy soil, the higher the conductivity, the more severe the attenuation of the electromagnetic wave, and the weaker the hyperbolic wrap-around wave energy. In the case of top leakage, the longer the leakage time, the larger the leakage area, the earlier the hyperbolic wrap-around wave appears, the weaker the energy, and the horizontal position of its apex remains unchanged; When the bottom leakage, there are two hyperbolic waves moving upward and downward, and the longer the leakage time, the weaker and more separated the two hyperbolic waves, and the horizontal position of their vertices remains unchanged; In the case of left (right) side leakage, the longer the leakage time, the weaker the energy of the hyperbolic wrap-around wave, the earlier the hyperbolic wrap-around wave appears, and the more the apex is shifted to the upper left (right). The simulation results can provide reliable technical support for the precise identification of water supply pipe leakage location and its leakage area.

Acknowledgements

Natural Science Foundation.

References

[1] X Gin: Electric field component imaging analysis of ground-penetrating radar data for pipeline leakage anomalies, Coalfield Geology and Exploration, vol. 46 (2018), 159-163.

[2] J Ji, J.C. Xia, Z.M. Zhang, et al. Numerical analysis of ground subsidence induced by sewage pipe leakage, Journal of Hohai University, vol. 49 (2021), 406-412.

[3] Y. C. Wang, H. H. Wang, P. J. Su, et al. Experimental analysis of ground-penetrating radar simulation for leakage detection of underground water supply pipes, Physical and chemical exploration vol. 47 (2023), 794-803.

[4] Z. F. Cao, S. F. Yang, S. R. Song, et al. Ground Penetrating Radar Data Processing Method and its Application. Geology Exploration, 32(1996), 34–42.

[5] Y. Shen, L. Y, P. Li, et al. Simulation and Detection Leakage of Underground Water Pipeline by Ground Penetrating Radar, Journal of Testing and Evaluation, vol. 48 (2019), 2003-2027.

[6] Lai W W L, Chang R K W, Sham J F C, et al. Perturbation mapping of water leak in buried water pipes via laboratory validation experiments with high-frequency ground penetrating radar (GPR), Tunnelling and Underground Space Technology, 52(2016), 157-167.

[7] Peter King-Wah Lau, Bella Wei-Yat Cheung, Wallace Wai-Lok Lai, Janet Fung-Chu Sham Characterizing pipe leakage with a combination of GPR wave velocity algorithms, Tunnelling and Underground Space Technology, 103740(2021): 1-12.

[8] H. T. Song, L. Gao, C. Han, et al. Geo-Radar Orthorectified Simulation Study of Underground Pipelines and Oil Spills, Energy and Environmental Protection,41(2019):52-57.

[9] Y. P. Sheng, S. H. Shu, Q. Wang, et al. Seepage modeling and ground-penetrating radar signal orthorectification for leakage in urban water supply pipelines, Journal of Engineering Geology, 24(2016):422-429 .

[10] Topp G C, Davis J L, Annan A P. Electromagnetic determination of soil water content: Measurements in coaxial transmission lines water content: Measurements in coaxial transmission lines, Water Resources Research, 16(1980):574-582.

[11] M. C. McCutcheon, H. J. Farahani, J. D. Stednick, G. W. Buchleiter, and T. R. Green, Effect of Soil Water on Apparent Soil Electrical Conductivity and Texture Relationships in a Dryland Field, Biosystems Engineering, 94(2006):19-32.